Korean J. Chem. Eng., 34(6), 1763-1773 (2017)
DOI: 10.1007/s11814-017-0080-7

pISSN: 0256-1115
eISSN: 1975-7220

Efficient pressure swing adsorption for improving H_2 recovery in precombustion CO_2 capture

Jehun Park, Rai H. Kang, and Jae W. Lee†

Department of Chemical and Biomolecular Engineering, Korea Advanced Institute of Science and Technology (KAIST), 291 Daehak-ro, Yuseong-gu, Daejeon 34141, Korea
(*Received 6 December 2016 • accepted 16 March 2017*)

Abstract−An efficient design for pressure swing adsorption (PSA) operations is introduced for CO_2 capture in the pre-combustion process to improve H_2 recovery and CO_2 purity at a low energy consumption. The proposed PSA sequence increases the H_2 recovery by introducing a purge step which uses a recycle of CO_2-rich stream and a pressure equalizing step. The H_2 recovery from the syngas can be increased over 98% by providing a sufficient purge flow of 48.8% of the initial syngas feeding rate. The bed size (375 m^3/(kmol CO_2/s)) and the energy consumption for the compression of recycled CO_2-rich gas (6 kW/(mol CO_2/s)) are much smaller than those of other PSA processes that have a CO_2 compression system to increase the product purity and recovery.

Keywords: CO_2 Capture, Pre-combustion Process, Pressure Swing Adsorption (PSA), H_2 Recovery, Purge Step, Pressure Equalizing Step

INTRODUCTION

Greenhouse gases such as CO_2 are well known for the main cause of global warming and there are various efforts for reducing greenhouse emissions [1]. The separation of CO_2 from the flue gas generated at the power plant can be applied to either post- or pre-combustion, depending on where the separation process is placed, as shown in Fig. 1 [2,3]. So far, more studies have been conducted on the separation of CO_2 from the post-combustion gas mixture than from the pre-combustion gas mixture, because the separation of CO_2 occurs after the final product of flue gas is collected; therefore, it does not affect the pre-existing operation unit. Contrary to this process, the pre-combustion method employs a water gas shift (WGS) reactor first, and it produces H_2 and CO_2 from the shift reaction of water and CO. The next step is the separation of CO_2 from the fuel gas before the gas enters into a combustion chamber so that the resultant, H_2-rich gas can be supplied to a combustion chamber.

Due to the difference in the separation of the CO_2 process, main components of the post-combustion gas are N_2 and CO_2, whereas those of the pre-combustion syngas are H_2 and CO_2. The post-combustion flue gas has atmospheric pressure or slightly higher pressure than 1 bar, while the pre-combustion gas stream has a pressure range of 20-30 bars. The low CO_2 partial pressure of flue

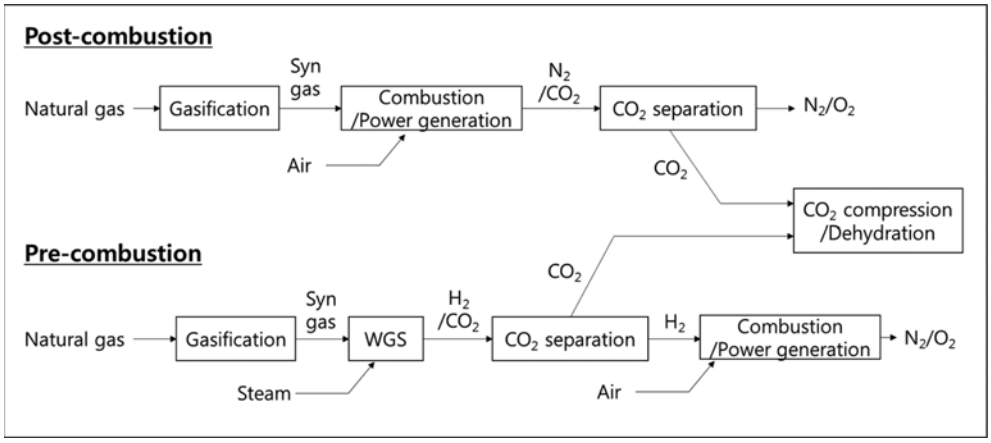

Fig. 1. Comparison of post-combustion and pre-combustion processes for carbon capture and sequestration (CCS).

†To whom correspondence should be addressed.
E-mail: jaewlee@kaist.ac.kr, jaelee43@gmail.com

gas (0.05-0.25 bar) in the post-combustion process could impose difficulties on developing new adsorbent-based CO_2 capture processes. In contrast, CO_2 has a high partial pressure (5-15 bars) in the pre-combustion syngas and this pressure range could be a sufficient driving force to apply a pressure swing adsorption (PSA) method for the separation of CO_2. However, the main disadvantage of CO_2 capture from the pre-combustion process is H_2 loss due to the incomplete recovery of H_2 in the CO_2 rich stream [4,5]. If we improved the H_2 recovery from the pre-combustion gas stream, it would be more beneficial for CO_2 capture in the pressure swing adsorption (PSA) process, while gaining additional power from the H_2 recovery in the plant. Various PSA operation schemes have been developed for improving the performance of gas adsorption and desorption, such as introduction of a purge step and/or pressure equalizing (EQ) step between beds. The PSA process is equipped with several beds in one group because there are transfers of gas between beds. Smith and Westerberg [6,7] suggested various PSA processes which consisted of two to five beds in a group and subdivided EQ steps. For each case, operating conditions such as pressure and step time were optimized. Doong and Yang [8] proposed a PSA process which includes EQ and purge steps for H_2 purification, and analyzed the PSA performance by varying the purge rate. Distinct characteristic of the PSA process sequence suggested in their study is that the H_2-rich gas stream was used not only for the purge step of the bed, but also for the pressurization step. Jiang et al. [9] introduced a PSA process for H_2 purification by optimizing operation conditions of time intervals of each step and flow rate.

Most of the PSA processes for CCS from the post-combustion gas stream are based on vacuum swing adsorption (VSA), where desorption of CO_2 occurs under a vacuum condition. Chaffe et al. [10] and Zhang et al. [11] carried out nine-step VSA operations having purge steps and six-step VSA operations without purge steps by using zeolite 13X as an adsorbent, and evaluated the VSA performance of the two design schemes. Kikkinides et al. [12] employed activated carbon (AC) as an adsorbent for the removal of CO_2 and utilized the separated CO_2-rich gas to purge another column by pressurizing the gas stream. Chue et al. [13] studied AC and zeolite 13X as adsorbents and evaluated the performance of the two adsorbents. They also used a purge step using the recycled CO_2 gas. Reynolds et al. [14,15] proposed complex PSA sequences having light and heavy reflux streams and carried out sensitivity analyses to find optimal operating conditions. Chou and Chen [16] proposed a PSA operation sequence using the CO_2-rich stream to purge the adsorption bed and compared the experimental and simulation results of the PSA operation. The PSA sequence introduced by Gomes and Yee [17] also used a purge step using the N_2-rich gas after the CO_2 blow down step. Different from the conventional type of processes, Hirose [18] and Leavitt [19] suggested a duplex PSA process be introduced. In this duplex process, two columns consist of a group of columns, having improved separation efficiency despite the low pressure difference between the two columns. Sivakumar and Rao [20] proposed a modified duplex PSA process that can separate main components of the post-combustion gas, CO_2 and N_2, with both high purity and recovery. Agarwal et al. [21] developed a two-bed PSA superstructure composing of co-current and counter-current beds. Each bed performed adsorption of CO_2 at a high pressure and desorption at a vacuum condition.

Our aim was to design new PSA operation sequences for the pre-combustion CO_2 capture process for the purpose of improving the H_2 recovery as well as minimizing the energy consumption. The proposed PSA operation sequences contain pressure equalizing and purge steps for the pre-combustion CO_2 capture process. A dynamic model was developed to predict the performance of the PSA process by adopting mass and heat balances implemented with effective porosity, and dynamic simulations of the proposed sequences were performed to find the most efficient PSA operation sequence for the enhanced H_2 recovery with a low energy input. Finally, the simulation results were compared with other results from the previous works [13,20,21], by mainly focusing on the energy consumption and bed size.

DYNAMIC MODELING WITH AN EFFECTIVE POROSITY

The modeling conditions such as adsorbent specification, column dimension, and feed flow rates were adopted from Schell et al. [22]. Thermodynamic properties of H_2 and CO_2 gases were obtained with the SR-POLAR method from ASPEN Properties^{TM}. The mass balance for each component in Eq. (2) is given by ignoring the radial dispersion,

$$\frac{\partial(v_g c_i)}{\partial z} + \varepsilon_i \frac{\partial c_i}{\partial t} + J_i = 0 \tag{1}$$

where c_i is a molar concentration of component i in the gas phase, ε_i is the inter-particle porosity and J_i is a mass transfer rate of component i. The linear driving force (LDF) model is used for the mass transfer rate as written below:

$$J_i = \rho_B \frac{\partial q_i}{\partial t} = k_i (q_i^* - q_i) \tag{2}$$

where ρ_B is an adsorbent bulk density, k_i is a mass transfer coefficient of component i, q_i is the concentration in the adsorbed phase and q_i^* is the concentration of each component at equilibrium state. The values of the model parameters including isotherm data are available from Casas et al. [23]. Further detailed information for these data is attached in the Supporting Information.

The energy balance equation for each component is given below:

$$C_{vg} v_g \rho_g \frac{\partial T_g}{\partial z} + (\rho_s C_{ps} + \varepsilon_B C_{vg} \rho_g) \frac{\partial T_g}{\partial t} + P \frac{\partial v_g}{\partial z} + \rho_s \sum_i \left(\Delta H_i \frac{\partial q_i}{\partial t} \right) + \frac{4 H_I}{D_I} (T_g - T_w) = 0 \tag{3}$$

where C_{vg} is the specific gas phase heat capacity at the constant volume, v_g and ρ_g are velocity and density of gas, respectively, ρ_s is a bulk density of a sorbent, C_{ps} is a specific heat capacity of the adsorbent, ε_B is the total bed porosity, T_g is the temperature of gas phase, P is the total pressure of the system, ΔH_i is the heat of adsorption of component i, H_I is a heat transfer coefficient between gas phase and wall, D_I is a tube inner diameter and T_W is the temperature of cooling agent. The mass transfer coefficients of H_2 and CO_2 are k_{CO_2}=0.15 s^{-1} and k_{H_2}=1.0 s^{-1}, respectively, with the heat transfer coefficient of (H_I) equal to 5 W/m^2K [23,24].

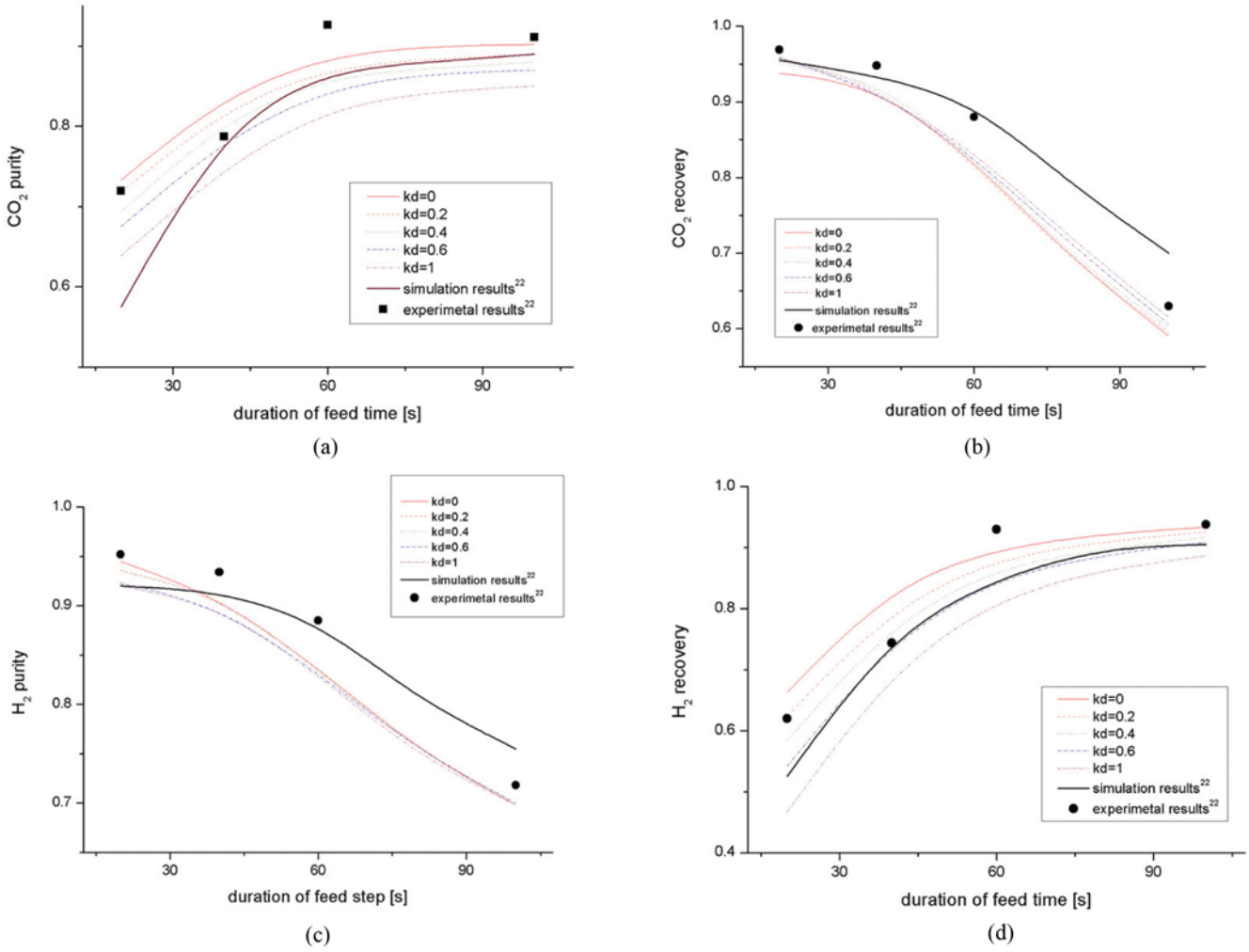

Fig. 2. Dynamic simulation results with the fraction of accessible pore volumes (K_d): (a) CO_2 purity, (b) CO_2 recovery, (c) H_2 purity and (d) H_2 recovery. The prior simulation and experimental results were employed from Schell et al. [22] for the comparison purpose.

The total bed porosity (ε_B) in Eq. (4) can be defined by considering both inter-particle porosity (ε_i) and intra-particle porosity (ε_p) [24,25].

$$\varepsilon_B=\varepsilon_i+\varepsilon_p(1-\varepsilon_i) \tag{4}$$

Therefore, the bed density (ρ_B) can be calculated as follows:

$$\rho_B=(1-\varepsilon_i)(1-\varepsilon_p)\rho_s+[\varepsilon_i+(1-\varepsilon_i)\varepsilon_p]\rho_g M_w \tag{5}$$

where ρ_B is the bed density, ρ_s is the structural solid density, ρ_g is the gas density and M_w is the mean molecular weight of the gas phase. Here, the effective bed porosity was used ($\varepsilon_{b,effective}$) by introducing K_d, the fraction of the pore volume that is accessible to the gas molecule.

$$\varepsilon_{B,effective}=\varepsilon_i+K_d\varepsilon_p(1-\varepsilon_i) \tag{6}$$

K_d is equal to 1, when the size of an adsorbent is sufficiently small and the adsorbate penetrates all pores of the adsorbent, while K_d is 0 when the size of the adsorbent is large and the adsorbate can penetrate none of the pores [25]. To solve the energy balance in Eq. (4), the insertion of an additional term considering the effective porosity is required. Using the model above with the varying K_d, we compared the previous experiment data [22] with our simulation results in terms of H_2/CO_2 recovery and purity defined as follows:

$$\begin{aligned}
&CO_2\ \text{Recovery}=\frac{\text{Amount of } CO_2 \text{ in the } CO_2\text{-rich gas}}{\text{Amount of total } CO_2 \text{ in the feed}}\\
&CO_2\ \text{Purity}=CO_2 \text{ mole fraction of the } CO_2\text{-rich gas}\\
&H_2\ \text{Recovery}=\frac{\text{Amount of } H_2 \text{ in the } H_2\text{-rich gas}}{\text{Amount of total } H_2 \text{ in the feed}}\\
&H_2\ \text{Purity}=H_2 \text{ mole fraction of the } H_2\text{-rich gas}
\end{aligned} \tag{7}$$

To conduct statistical analyses, we adopted the least square method (LSM) to determine the summation of square of errors (SSE) as in Table 1. The model had the highest accuracy with a value of K_d

Table 1. Results from the least square method (LSM)

	Results of this study					Previous simulation results [22]
K_d	0	0.2	0.4	0.6	1	
SSE	0.0258	0.0195	0.0209	0.0324	0.0727	0.0497

equal to 0.2, which case provided the closest estimation to the experimental data.

DESIGN OF PSA SEQUENCES FOR CCS FROM THE PRE-COMBUSTION PROCESS

Loss of H_2 deteriorates the total efficiency of the combined cycle process because H_2 is the valuable fuel in the combustion chamber and it releases 286 kJ per mole by the following reaction,

$$H_2+0.5\ O_2 \rightarrow H_2O \quad \Delta H=-286\ kJ/mol \tag{8}$$

Thus, improving the recovery of H_2 is one of the important factors to increase the efficiency in the CCS in the pre-combustion process. The other important factor is to achieve a high CO_2 purity because CO_2 recovered from the PSA process should be used as a feedstock to other chemical processes or to be captured and stored.

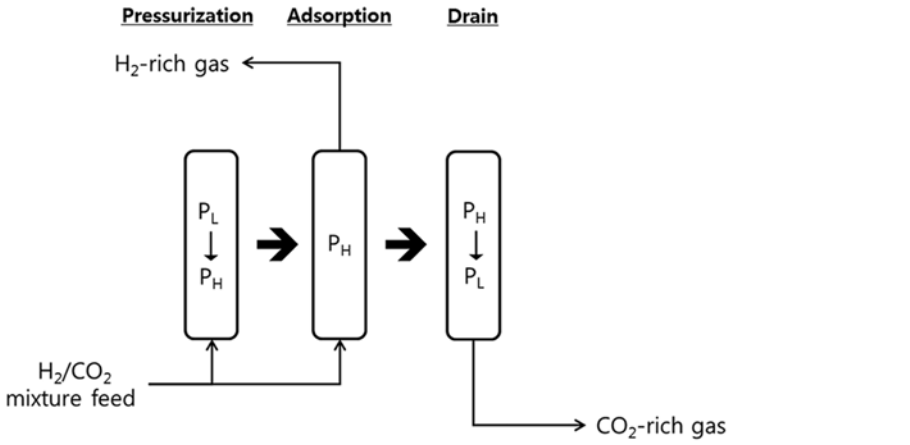

Column 1	P-up	Adsorption	Drain	
Column 2	Drain		P-up	Adsorption
Duration	45s	60s	45s	60s

(a) Case 1: Simple PSA operation with pressurization, adsorption and drain.

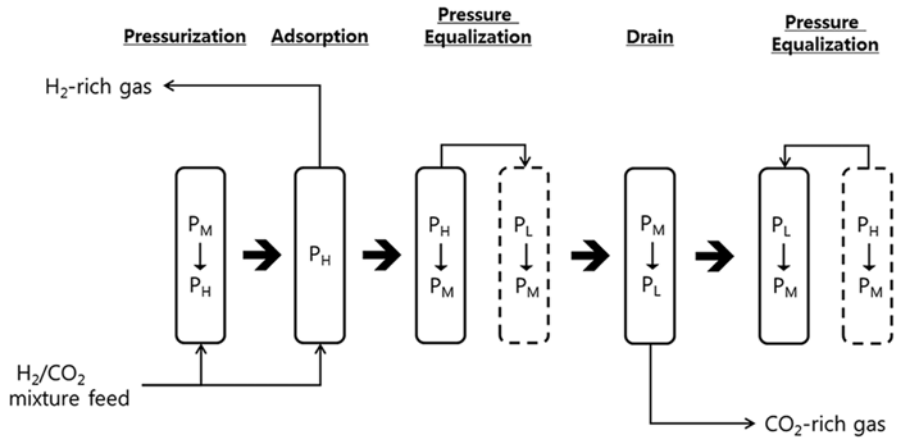

Column 1	P-up	Adsorption	EQ	Drain		EQ
Column 2	Drain		EQ	P-up	Adsorption	EQ
Duration	25s	60s	5s	25s	60s	5s

(b) Case 2: Alternative PSA sequence with an additional pressure equalizing (EQ) step.

Fig. 3. Five PSA design alternatives for CCS from the pre-combustion process. The high pressure condition (P_H) was set to 21 bars and the low pressure condition (P_L) was set to 1 bar for all of the cases. After the EQ step, the equalizing pressure (P_M) is around 7-9 bars and its variation is dependent on the desorbed gas composition.

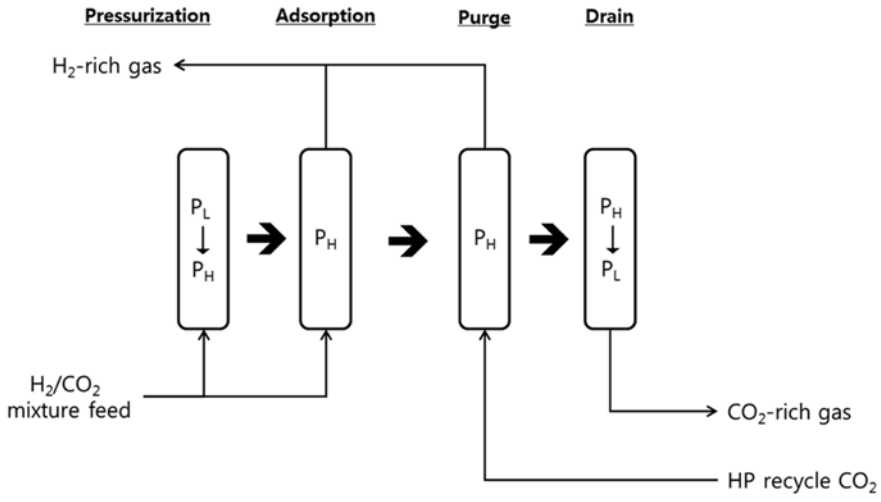

Column 1	P-up	Adsorption	Purge		Drain	
Column 2	Drain		P-up	Adsorption	Purge	
Column 3	Purge		Drain		P-up	Adsorption
Duration	45s	60s	45s	60s	45s	60s

(c) Case 3: Alternative PSA sequence with an additional purge step.

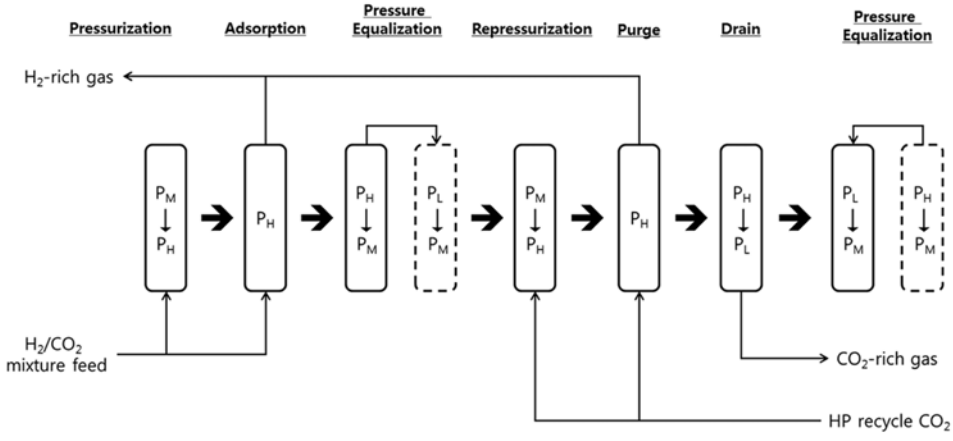

Column 1	P-up	Adsorption		EQ	P-up for purge		Purge		Drain			EQ		
Column 2	P-up for purge		Purge		Drain			EQ	P-up	Adsorption		EQ		
Column 3	Drain			EQ	P-up	Adsorption		EQ	P-up for purge		Purge			
Duration	45s	(60-τ)s	τs	5s	45s	(60-τ)s	τs	5s	45s	(60-τ)s	τs	5s		

(d) Case 4: Alternative PSA sequences with EQ and purge steps.

Fig. 3. Continued.

Since the major gaseous components in the pre-combustion process are H_2 and CO_2, the more H_2 that is recovered in the H_2-rich stream from the bed, the higher CO_2 purity will be achieved. Generally, the range of the syngas pressure is between 20 and 30 bars and by varying the pressure, the adsorption of the syngas is assumed to occur at 21 bars using the pressure of the syngas, while the desorption process occurs at 1 bar. As a result, some portion of the gas will remain in the bed because the desorption process does

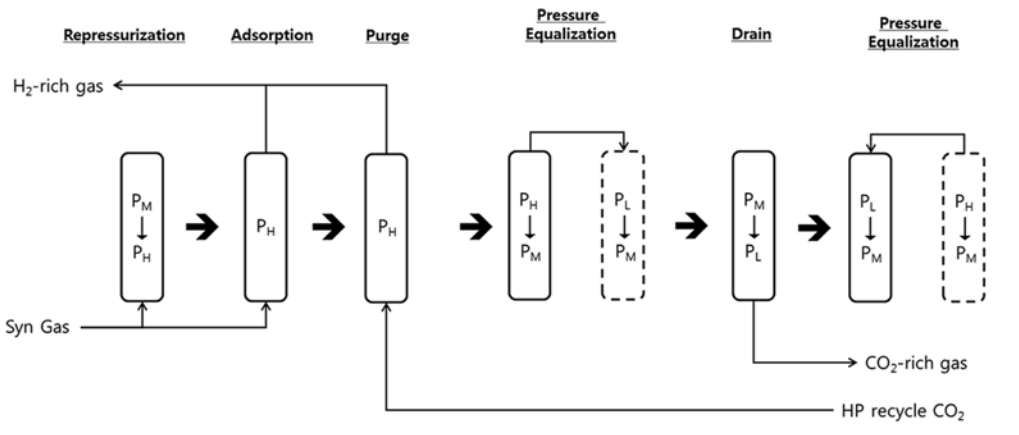

Column 1	P-up	Adsorption			Purge		EQ	Drain			EQ
Column 2	Purge			EQ	Drain		EQ	P-up	Adsorption		
Column 3	Drain			EQ	P-up	Adsorption			Purge		EQ
Duration	25s	55s	5s		25s	55s	5s	25s	55s		5s

(e) Case 5: Alternative PSA sequence with purge and EQ steps.

Fig. 3. Continued.

not take place at a perfect vacuum condition. Therefore, to improve the H_2 recovery, we introduced both a purge step at 21 bars and pressure equalizing (EQ) step at 7-9 bars to the cyclic operation for the CO_2 capture of the pre-combustion process.

In Fig. 3, we propose several PSA design alternatives for the CO_2 capture of the pre-combustion process and account for a cyclic operation sequence of one column. One exception is that the bed of dotted line represents another column connected with the bed of solid line at the EQ step. Descriptions of each step are as follows: 1) The pressurization before the adsorption step is to increase the bed pressure to a preset value for a desired adsorption condition by utilizing the syngas pressure. 2) The adsorption step involves CO_2 adsorption of the syngas in the column bed. 3) The drain step is to vent out the CO_2-rich gas stream as a product from the bed. The gas pressure must be released in the counter-current direction to prevent break-through of impurities existing at the top of the adsorber. 4) The EQ step brings pressure synchronization by opening the valve which connects one column having a high pressure with the other column having an atmospheric pressure after the drain step. 5) The purge step is to send residual H_2 in the bed after the adsorption step to the combustion chamber. In this step, the separated CO_2-rich stream is compressed and recycled to the column as a purge stream. 6) The repressurization for the purge step is used only in Case 4 (as explained below) to increase the bed pressure by recycling the CO_2-rich stream.

Case 1 is the simplest PSA operation where a single column continuously repeats the sequence including the pressurization, the adsorption and the drain steps [26]. Cases 2-5 are the alternative PSA designs to evaluate the effect of the additional EQ and purge steps. Only either the EQ step or the purge step is added to case 2 or 3, respectively. Both EQ and purge steps are employed in cases 4 and 5. The sequence of EQ-then-Purge in case 4 is almost identical to the sequence in Na et al. [27] but the sequence in case 5 is changed to purge-then-EQ. For cases 3-5, the CO_2 rich gas product is recycled as a purge gas instead of the H_2-rich gas stream. It aims to prevent the H_2 loss in the purge step and to enhance both H_2 recovery from the bed and additional CO_2 adsorption onto the bed. The detailed explanation for this choice of CO-rich gas heavy reflux is given in the Supporting Information.

To carry out comparative studies on the performance of each case under the same conditions, the following initial conditions are assumed: each design alternative has 12.3 mmol/s of syngas feed having an equimolar mixture of H_2 and CO_2. All beds have identical dimensions of 1.2 m in the length and 0.025 m in the internal diameter. The K_d value is set to equal to 0.2, which is the same as that obtained from the previous section. Durations of the adsorption and EQ steps are as 60 s and 5 s for each case, respectively. The pressurization step for adsorption takes 25 s with the EQ step but 45 s is required to increase pressure without the EQ step. The duration of pressurization in case 4 varies according to the flowrate of the purge gas stream. For example, if the flowrates of the recycled CO_2 rich-gas are 4, 5 are 7 mmol/s, the duration of pressurization for purge are 85, 65 and 50 s, respectively. Figs. 4-6 show the simulation results that both CO_2 purity and H_2 recovery are improved with EQ and purge steps, respectively. Both purge and EQ steps increase the H_2 recovery, but there are significant differences of their effect on the recovery depending on the sequence of these two steps applied. With an additional EQ step, the H_2 gas remaining within the pore of the high pressure bed is transferred to another low pressure column. In this process, the amount of the transferred H_2 is proportional to the pressure change of the bed and the H_2 removal is rapidly done throughout the entire bed as

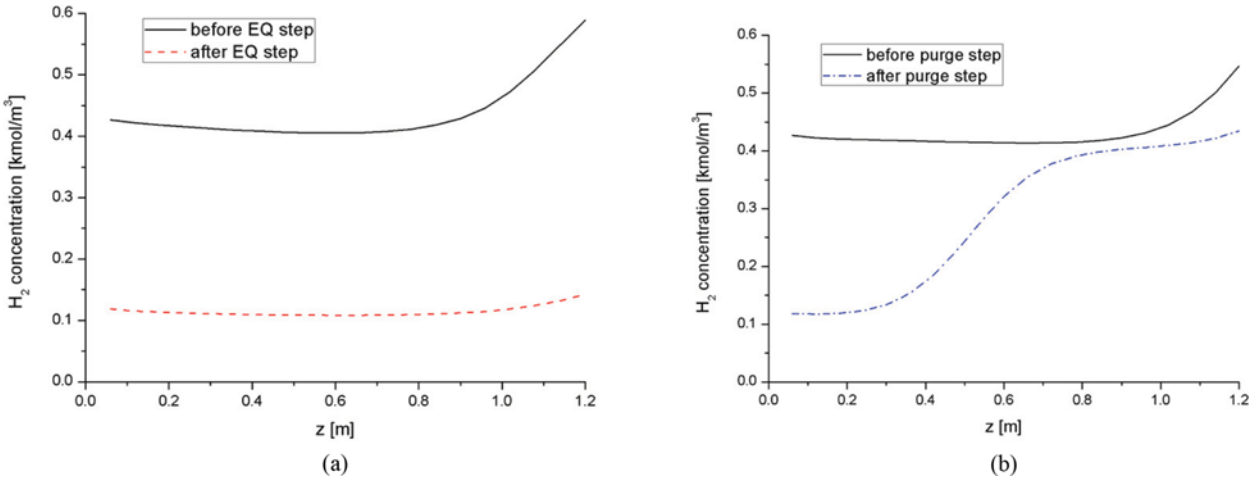

Fig. 4. H_2 concentration along the bed height, z (z=0 at the bottom and z=1.2 at the top) before and after the EQ or the purge step. (a) H_2 concentration before and after the EQ step in Case 2. (b) H_2 concentration before and after the purge step in Case 3.

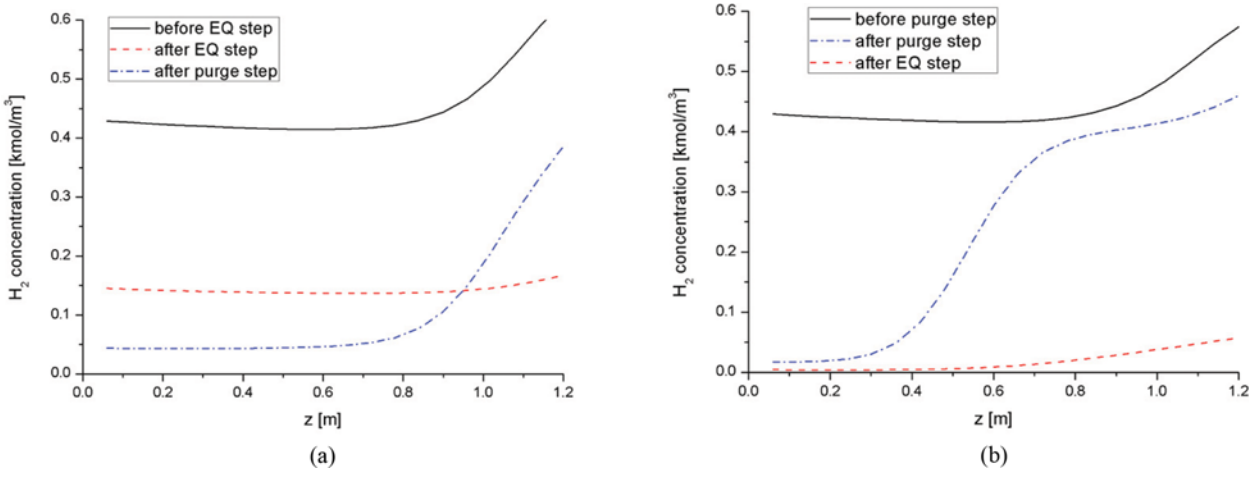

Fig. 5. H_2 concentration in the bed from different sequences of EQ and purge steps. (a) H_2 concentration according to the bed position in Case 4. (b) H_2 concentration according to the bed position in Case 5.

shown in Fig. 4(a).

However, the purge step uses the recycled CO_2-rich gas containing a relatively high fraction of H_2 (15%) at a total pressure of 21 bars, which can contribute to the high H_2 concentration at the end of the bed. Furthermore, the H_2 removal is conducted gradually from the bottom part of the column where the purge gas enters. Although the feeding rate of the recycled CO_2-rich gas is high (5 mmol/s), the H_2 concentration near the outlet is still high even after the purge step as shown in Fig. 4(b). If both EQ and purge steps are employed, then the operation sequence of these two steps significantly affects the H_2 recovery. For this reason, cases 4 (EQ-then-purge) and 5 (purge-then-EQ) have in the different sequence.

The H_2 concentration after both steps does not get lower in case 4 in comparison to case 5 as shown in Fig. 5. However, the H_2 concentration is further reduced after the EQ step in case 5 because H_2 is first desorbed and emitted by the CO_2-rich gas stream at the purge step and then its concentration gets again lowered by the pressure drop at the EQ step. The differences of both CO_2 purity and H_2 recovery are reflected in Fig. 6 for the five cases. If only one step is applied between EQ and purge steps such as in cases 2 and 3, the EQ step has greater influence on improving the H_2

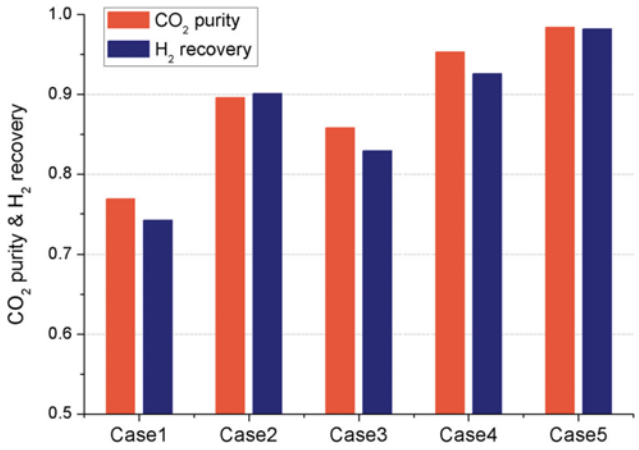

Fig. 6. CO_2 purity and H_2 recovery for each PSA design.

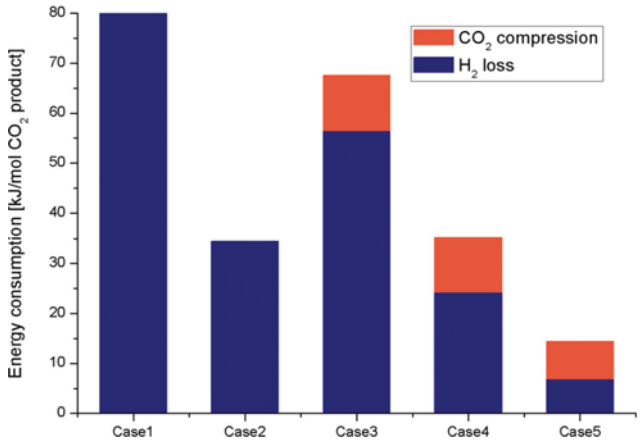

Fig. 7. Energy consumption for each PSA sequence design.

Table 2. Conditions for recycled CO_2-rich gas compression

	Value
Number of inter-cooled stages	3
Inter-cooling temperature (°C)	60
Inter-coolers pressure loss (%)	1
First compressor inlet pressure (bar)	1
Last compressor outlet pressure (bar)	22
Isentropic/Mech.-electric efficiency of compressors (%)	82/94

recovery. If both EQ and purge steps are employed, the purge-EQ sequence in case 5 shows much higher CO_2 purity and H_2 recovery than the EQ-purge sequence in case 4. More complex PSA sequences with multiple reflux purge streams [14,15] were proposed to improve the performance, but the complex design can lead to increasing bed sizes, investment and operating costs. The detailed analyses for the bed size calculation are given in the Supporting Information.

The total energy consumption of each case is determined as shown in Fig. 7 in terms of H_2 loss and CO_2 compression energy. Approximately, 11.8 kJ is required to compress 1 mole of CO_2. The H_2 loss is translated into a heat loss that is equal to 286 kJ per mole of H_2. Additionally, the PSA sequences of cases 3-5 use the recycled CO_2-rich gas as the purge gas and need its compression to increase the purge gas pressure. With conditions suggested in Table 2, the required CO_2 compression energy for the purge step was calculated. As shown in Fig. 7, case 5 is the most energy efficient PSA operation sequence. The following section provides further sensitivity analyses for case 5 alone.

SENSITIVITY ANALYSIS ABOUT THE PSA PERFORMANCE WITH VARYING PURGING RATES

The performance of the PSA operation (case 5) was estimated by changing the purge rate with the fixed time duration for all steps in the operation sequence. The recycle purge rate and CO_2 purity of the CO_2-rich gas are given in Table 3. The purge rate varies from 0.5 to 4.0 mmol/s and it corresponds to 8.1% to 65.5% of the CO_2 molar flow rate in the syngas feed. Fig. 8 shows the H_2 fraction of the gas phase at different column positions during the purge

Table 3. Purge rate and CO_2 purity of the CO_2-rich gas

Purge gas rates (mmol/s) and purge gas CO_2 purity (mole fraction)				
0.5	1.0	2.0	3.0	4.0
0.91	0.93	0.96	0.98	0.99

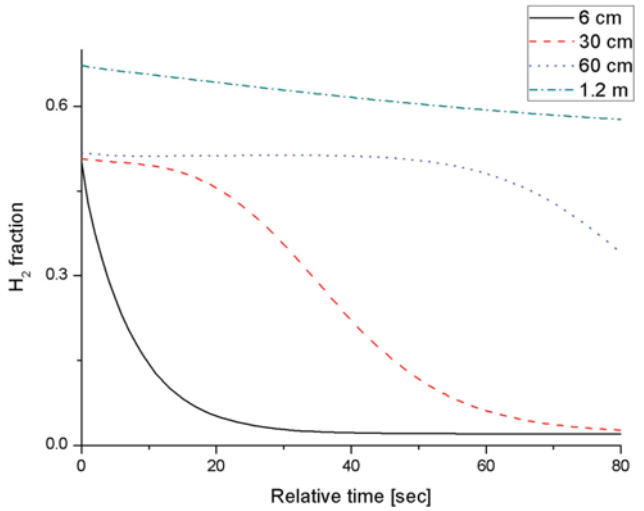

Fig. 8. H_2 fraction in the gas phase depending on the column bed position (Purge rate=3 mmol/sec).

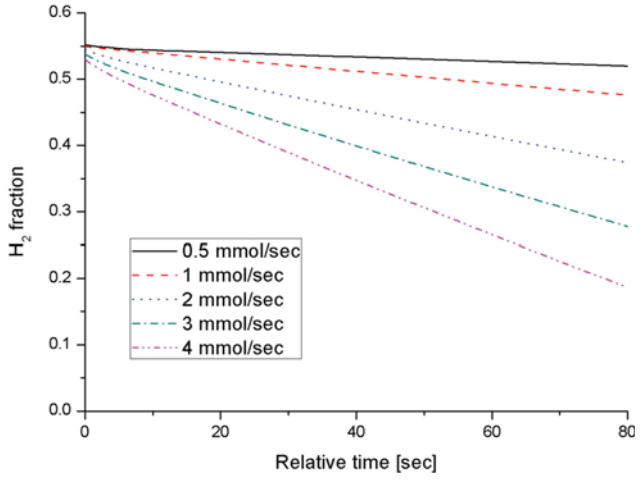

Fig. 9. Changes of H_2 fraction in the gas phase depending on the purge rate.

step when the purge rate is 3 mmol/s. The H_2 fraction decreases rapidly at the inlet position of the bed (0 m). However, there is almost no change in the concentration at the outlet of the bed (1.2 m).

When we calculate the H_2 mole fraction of the entire bed, it is 0.3 after the completion of the purge step with the purge rate of 3 mmol/s in Fig. 9. Fig. 9 indicates that the H_2 concentration at the gas phase decreases with the time, but the CO_2 concentration at the gas phase increases as the purge rate is rising. The H_2 fraction decreases below 0.2 when the purge rate increases to 4 mmol/s. Also, almost no change in the H_2 fraction is observed when the purge rate is 0.5 mmol/s. However, the H_2 purity gets lower with

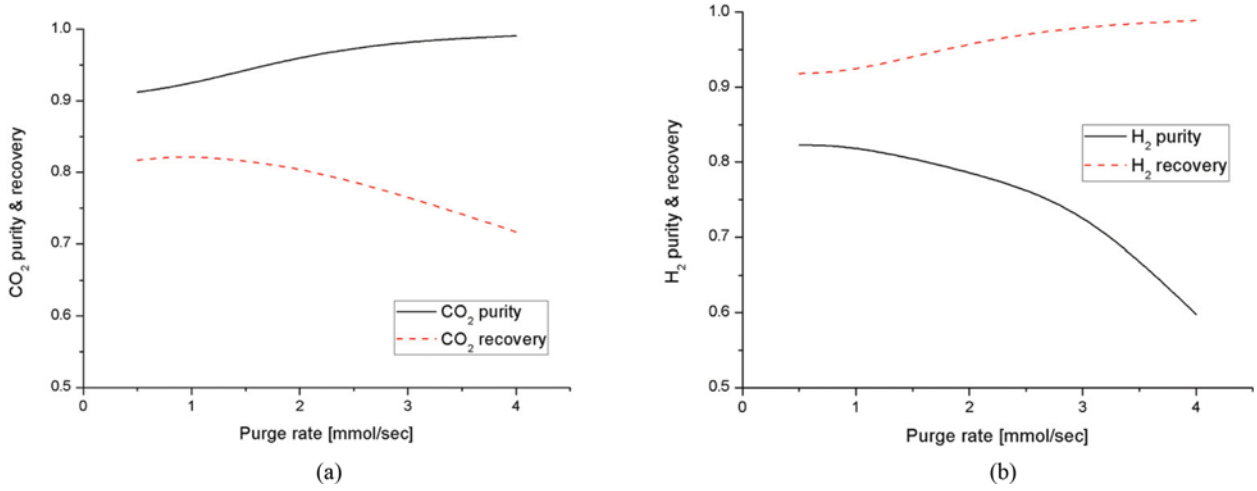

Fig. 10. Sensitivity analyses of (a) CO_2 recovery and purity, (b) H_2 recovery and purity in Case 5 with the varying purge rate.

the increasing purge rate due to the influx of CO_2 into the H_2-rich gas even if both H_2 recovery and CO_2 purity can be improved by the purge step.

Fig. 10 shows the calculation result of CO_2 purity and H_2 recovery with various purge rates. There is a tendency that increasing the purge rate leads to higher CO_2 purity (Fig. 10(a)) and H_2 recovery (Fig. 10(b)) while lowering both CO_2 recovery and H_2 purity. When the purge rate is above 3 mmol/s, the H_2 recovery is improved to higher than 0.98 and the loss of H_2 fuel decreases remarkably. However, further increasing the purge rate causes more energy consumption for the compression of recycled CO_2-rich gas. Therefore, for the following economic assessment section, the calculation of the compression energy consumption and the H_2 fuel loss was performed by converting both compression work and H_2 loss into the energy requirement. When the purge rate is 0.5 mmol/s, 25.7 kJ of heat/energy is lost to separate 1 mole of CO_2 which is equivalent to 8% of entire H_2 fuel (Fig. 11). When the purge rate increases to 3 mmol/s, the electrical energy of 6 kJ/mol CO_2 is required but the H_2 fuel loss decreases drastically down to 5 kJ/mol CO_2. Increasing the purge rate above this level causes the compression energy consumption to become larger than the energy gain from the reduction of H_2 fuel loss.

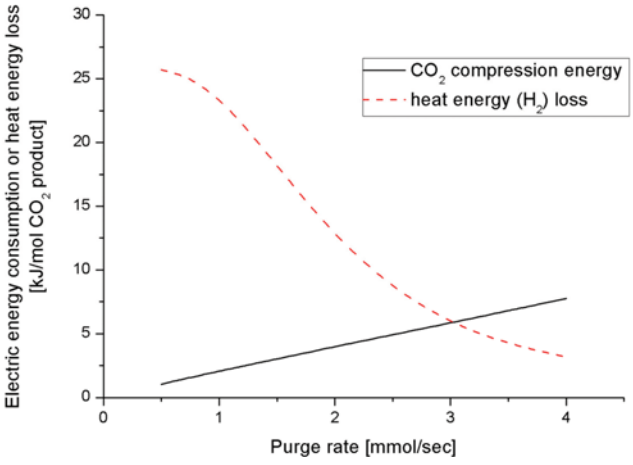

Fig. 11. Energy requirement for the compression of CO_2-rich gas and the heat energy loss (H_2 loss) for CCS in the pre-combustion process.

ECONOMIC ASSESSMENT

Table 4 presents both energy consumption and bed volume, which are the main factors for determining investment and operating costs. Because there have been very few studies for CO_2 capture from the pre-combustion process, we compared the results with the prior studies [13,20,21] regarding the post-combustion process. For a fair comparison, however, we took an additional energy penalty of 5 kJ/mol CO_2 into account in the assessment due to the H_2 fuel loss that was the optimal case with a purge rate of 3 mmol/

Table 4. Comparative performance of each PSA sequence design

	Duration time		CO_2 flow rate	PSA performance		Required volume	Energy consumption
	Total	Feeding		CO_2 purity	CO_2 recovery		
	s	s	mmol/s	-	-	m^3/(kmol CO_2/s)	kW/(mol CO_2/s)
This study	255	255	6.15	0.984	0.766	375	6 (+5 H_2 loss)
Chue et al. [10]	420	417	2.71	0.999	0.74	751	-
Original Duplex [20]	50	40	1	0.77	0.77	1594	31.2
Modified Duplex [20]	54	40	1	0.995	0.995	1332	107.8
Agarwal et al. [21]	2400	2343	-	0.90	0.85	554	73.6

s as shown in Fig. 11.

Chue et al. [13] used a discharging pressure of CO_2 equal to 50 mmHg (~0.065 bar) because of their use of the post-combustion gas as a feed gas for the PSA process, and this condition can be viewed as a vacuum condition. Their PSA sequence has a distinct form where the CO_2-rich product gas is recycled as a purging gas of the following columns. In line with the result of the current study, they showed that the purge brought about the increment of CO_2 purity but did not improve the CO_2 recovery. For a higher purity of CO_2 (0.999) than that (0.984) in this study, a larger size of bed is necessary to separate the same amount of CO_2 in the PSA process using the post-combustion gas (751 m^3/(kmol CO_2/s)) than in the PSA process using the pre-combustion gas (375 m^3/(kmol CO_2/s)) as shown in Table 4.

The original duplex PSA process has a pair of columns that have adsorption at one column with a high pressure and desorption with the other column simultaneously with a low pressure. The flue gas feed is injected to the middle of the high pressure column. Also, both outlets of one column become the inlet of the other, so enormous compression energy is required when the outlet of a low pressure column is going to be the inlet of a high pressure column. The modified duplex PSA is proposed by Sivakumar and Rao [20] to separate the gas product sharply. Different from the original duplex PSA operation sequence, adsorption and desorption process do not occur simultaneously, which improves both CO_2 purity and CO_2 recovery. But both duplex processes still require high energy consumption and bed size. For example, in the original duplex case, both energy requirement and bed size are 31.2 kW/(mol CO_2/s) and 1,594 m^3/(kmol CO_2/s), respectively, as shown in Table 4 for the same CO_2 recovery (0.77) and lower CO_2 purity (0.77) compared to those (0.766 and 0.984) in this study.

A comprehensive study for increasing the volumetric flow rate of CO_2 with the same bed size [21] showed a significant reduction in the bed size and energy consumption (554 m^3/(kmol CO_2/s) and 73.6 kW/(mol CO_2/s)) compared to the modified duplex case. The energy consumption is still large for higher CO_2 recovery (0.85) and lower CO_2 purity (0.90) than those (0.766 and 0.984) in this study. Hence, although the PSA process in this study has low CO_2 recovery, the proposed design shows advantages in having both low energy consumption with the high H_2 recovery (98% in Fig. 10(b)) and the small bed size when compared to the other PSA processes as shown in Table 4.

CONCLUSION

We have proposed design alternatives of the PSA operation sequence to capture CO_2 from the pre-combustion process. Particularly, we focused on improving the H_2 recovery of the fuel gas and the CO_2 purity of the separated CO_2-rich gas to be transported or stored after the compression. Several design alternatives of the PSA operation sequence were generated and the performance of each alternative was compared. Introducing both purge step and pressure equalizing step is essential to improve both the H_2 recovery and CO_2 purity, and the performance is even much better when the sequence of purge and pressure equalizing steps is applied than the reverse sequence of the two steps. As a result, H_2 recovery can be achieved above 98%. The new PSA operation provides both smaller bed size and less energy for compression than the other PSA designs for CCS from the post-combustion process.

ACKNOWLEDGEMENTS

The authors are grateful for the financial support from both Korea CCS R & D Center and UK-Korea Joint Research Program through NRF grants (NRF-2014M1A8A1049297 and NRF-2015M2A7A1000219) funded by the Ministry of Science, ICT, and Future Planning.

SUPPORTING INFORMATION

Additional information as noted in the text. This information is available via the Internet at http://www.springer.com/chemistry/journal/11814.

NOMENCLATURE

a_p : the specific particle surface area per unit volume bed [m^2 particle/m^3 bed]
c_i : molar concentration of component i [kmol/m^3]
C_{ps} : specific heat capacity of the adsorbent [MJ/kg·K]
C_{vg} : specific gas phase heat capacity at the constant volume [MJ/kmol·K]
ΔH_i : heat of adsorption of component i [MJ/kmol]
H_I : heat transfer coefficient between the gas phase and wall [MW/m^2·K]
H_S : heat transfer coefficient between the solid phase and gas phase [MW/m^2·K]
J_i : mass transfer rate of component I to adsorbent [kmol/m^3 bed·s]
k_i : mass transfer coefficient of component i [1/s]
K_d : fraction of volume of pores which a molecule can penetrates [-]
M_w : mean molecular weight [kg/kmol]
P : total pressure of this system [bars]
q_i^* : pure component loading of component i [kmol/kg]
q_i : loading of component i [kmol/kg]
T_g : gas phase temperature [K]
T_s : solid phase temperature [K]
v_g : gas velocity [m/s]

Greek Letters

ε_i : interparticle porosity [-]
ε_p : intraparticle porosity [-]
ε_B : bed porosity [-]
ρ_B : bed density [kg/m^3]
ρ_g : gas density [kmol/m^3]
ρ_s : structural solid density [kg/m^3]

REFERENCES

1. M. C. Romano, P. Chiesa and G. Lozza, *Int. J. Greenhouse Gas Control*, **4**, 785 (2010).

2. J. D. Figueroa, T. Fout, S. Plasynski, H. McIlvried and R. D. Srivastava, *Int. J. Greenhouse Gas Control*, **2**, 9 (2008).
3. M. Kanniche, R. Gros-Bonnivard, P. Jaud, J. Valle-Marcos, J. Amann and C. Bouallou, *Appl. Therm. Eng.*, **30**, 53 (2010).
4. S. Vora, L. Brickett, P. Indrikanti, R. Munson, J. Murphy, T. Rife, J. Strock and C. Zaremsky, *DOE/NETL advanced carbon dioxide capture R&D program: Technology update* (2013).
5. R. M. Davidson, *Pre-combustion capture of CO_2 in IGCC plants*, IEA Clean Coal Centre (2011).
6. O. J. Smith IV and A. W. Westerberg, *Chem. Eng. Sci.*, **46**, 2967 (1991).
7. O. J. Smith IV and A. W. Westerberg, *Chem. Eng. Sci.*, **47**, 4213 (1992).
8. S. J. Doong and R. T. Yang, *Reactive Polymers*, **6**, 7 (1987).
9. L. Jiang, V. G. Fox and L. T. Biegler, *AIChE J.*, **50**, 2904 (2004).
10. A. L. Chaffe, G. P. Knowles, Z. Liang, J. Zhang, P. Xiao and P. A. Webley, *Int. J. Greenhouse Gas Control*, **1**, 11 (2007).
11. J. Zhang, P. A. Webley and P. Xiao, *Energy Convers. Manage.*, **49**, 346 (2008).
12. E. S. Kikkinides, R. T. Yang and S. H. Cho, *Ind. Eng. Chem. Res.*, **32**, 2714 (1993).
13. K. T. Chue, J. N. Kim, Y. J. Yoo, S. H. Cho and R. T. Yang, *Ind. Eng. Chem. Res.*, **34**, 591 (1995).
14. S. P. Reynolds, A. D. Ebner and J. A. Ritter, *Ind. Eng. Chem. Res.*, **45**, 4278 (2006).
15. S. P. Reynolds, A. D. Ebner and J. A. Ritter, *Adsorption*, **14**, 399 (2008).
16. C. Chou and C. Chen, *Sep. Purif. Technol.*, **39**, 51 (2004).
17. V. G. Gomes and K. W. K. Yee, *Sep. Purif. Technol.*, **28**, 161 (2002).
18. T. Hirose, *Proceedings of the 2nd China-Japan-USA Symposium on Adsorption*, 123 (1991).
19. F. W. Leavitt, US Patent, 5,085,674 (1992).
20. S. V. Sivakumar and D. P. Rao, *Ind. Eng. Chem. Res.*, **50**, 3426 (2011).
21. A. Agarwal, L. T. Biegler and S. E. Zitney, *AIChE J.*, **56**, 1813 (2010).
22. J. Schell, N. Casas, D. Marx and M. Mazzotti, *Ind. Eng. Chem. Res.*, **52**, 8311 (2013).
23. N. Casas, J. Schell, R. Pini and M. Mazzotti, *Adsorption*, **18**, 143 (2012).
24. J. Park and J. W. Lee, *Korean J. Chem. Eng.*, **33**, 438 (2016).
25. P. C. Wankat, *Rate-controlled separations*, Elsevier Applied Science (1990).
26. A. Saberimoghaddam and A. Nozari, *Korean J. Chem. Eng.*, **34**(3), 822 (2017).
27. B.-K. Na, K.-K. Koo, H.-M. Eum, H. Lee and H. K. Song, *Korean J. Chem. Eng.*, **18**, 220 (2001).

Supporting Information

Efficient pressure swing adsorption for improving H_2 recovery in precombustion CO_2 capture

Jehun Park, Rai H. Kang, and Jae W. Lee†

Department of Chemical and Biomolecular Engineering, Korea Advanced Institute of Science and Technology (KAIST), 291 Daehak-ro, Yuseong-gu, Daejeon 34141, Korea
(*Received 6 December 2016 • accepted 16 March 2017*)

S1. Summary of Modeling Basis and Parameters

To calculate an adsorbed amount of H_2 and CO_2 gas on AC, we used the following adsorption model. The model is Sips equation and adopted from Casas et al. [23] with the parameters shown in Table S1

$$q_i^* = \frac{q_{si}(K_i p_i)^{s_i}}{1+\Sigma_{j=1}^{n}(K_j p_i)^{s_j}}$$

$$q_{si} = \omega_i \exp\left(\frac{-\theta_i}{RT}\right)$$

$$K_i = \Omega_i \exp\left(\frac{-\theta_i}{RT}\right)$$

$$s_i = s_{1i}\tan^{-1}(s_{2i}(T - T_{ref,i})) + s_{ref,i}$$

where q_i^* is the solid phase concentration of i component at equilibrium, p_i is the partial pressure of component i, T is the temperature, q_{si} and K_i are the saturation capacity and the adsorption equilibrium constant of component i and S_i is the homogeneity index of component i.

Schell et al. [22] experimentally constructed PSA operation se-

Table S1. Parameters for Sips isotherm model

			Unit	CO_2	H_2
q_{si}	[mol/kg]	ω_i	[mol/kg]	1.38	6.66
		θ_i	[J/mol]	−5628	0
K_i	[1/Pa]	Ω_i	[1/Pa]	16.80×10^{-9}	0.70×10^{-9}
		Θ_i	[J/mol]	−9159	−9826
s_i	[-]	s_{1i}	[-]	0.072	0
		s_{2i}	[1/K]	0.106	0
		$T_{ref,i}$	[K]	329	273
		$S_{ref,i}$	[-]	0.827	0.9556

Table S2. Column dimension and physical properties of adsorbent

	Symbol	Unit	Value
Column length	L	m	1.2
Internal diameter	D_I	m	0.025
External diameter	D_o	m	0.04
Heat capacity of wall	C_{pw}	J/K·m^3	4×10^6
Structural density	ρ_s	kg/m^3	1965
Particle density	ρ_p	kg/m^3	850
Bed density	ρ_B	kg/m^3	480
Particle diameter	d_p	m	0.003
Heat capacity of adsorbent	C_{ps}	J/K·kg	1000

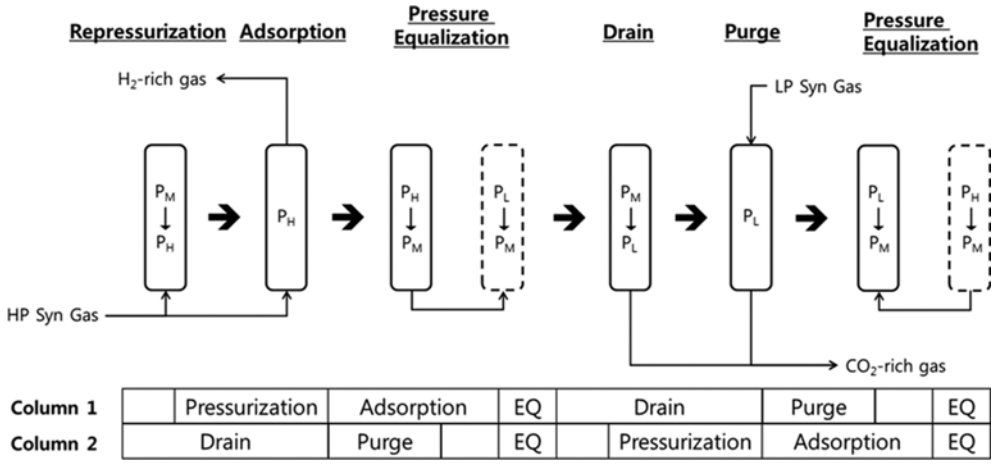

Fig. S1. PSA operation sequence proposed by Schell et al. [22].

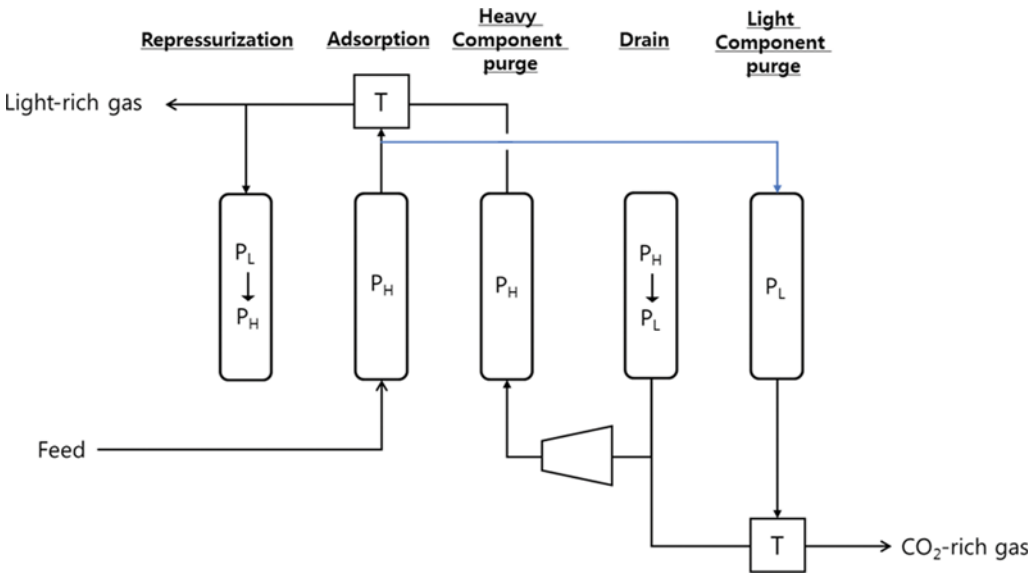

Fig. S2. Light gas external purge (modified from Fig. 1(d) in Reynolds et al. [14]).

quences as follows. More particularly, the process operates with one group of column consisting of 2 columns as a pair. The column dimension and physical properties of adsorbent are summarized in Table S2. Their PSA operation sequence is described in Fig. S1. Each column performs a sequence of re-pressurization, adsorption, pressure equalization, drain, purge and pressure equalization step repeatedly. From their experiment, the time required for each step is 24 s for re-pressurization, 3 s for pressure equalization, 50 s for drain, 15 s for purge, and varies from 20 to 100 s for the adsorption step.

S2. Choice of Heavy Gas (CO_2-rich Gas) as a Recycle Purge in the Pre-combustion CCS

There were two ways of purge by using a light gas [14,15], which could be an external purge or a reflux stream to another bed. Both are not effective in case of CCS for the pre-combustion process. First, if H_2-rich gas is used as a purge gas (blue line in Fig. S2) at the drain step like the external purge [14], it causes a serious H_2 loss in the pre-combustion CCS process.

If the light component gas (blue line in Fig. S3) is intended to be reused as a purge gas (red line) to another bed as shown in Fig. S3 [15], the CO_2 fraction of heavy reflux gas (red line) should be higher than that of original feed gas at the adsorption step. Only in this case, more CO_2 can be adsorbed and the other gas (H_2 in the pre-combustion CCS process) is desorbed from the bed after the adsorption step. Our proposed design uses the CO_2-rich gas whose CO_2 purity is above 95% as a heavy reflux purge gas and is higher than the CO_2 fraction in the feed gas (30-50%), thus the heavy reflux gas can make H_2 component more desorbed and CO_2 more ad-

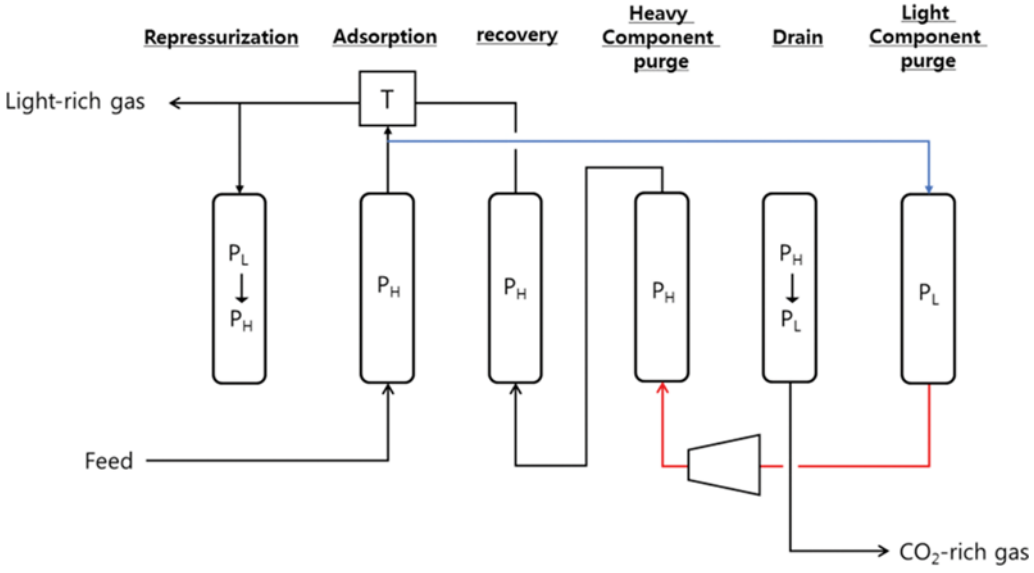

Fig. S3. Light gas recycle purge (modified from Reynolds et al. [15]).

sorbed at the purge step, which leads to higher H_2 recovery.

S3. The Minimum Bed Size Required for the Drain Step and the Feeding Step

To the best of our knowledge, there have been limited studies on determining the bed size in the PSA design. Here, we proposed the following method to calculate the minimum bed size required for the drain step and the feeding step. From the calculations, we can figure out which factor is a main contributor to the bed size increase.

First, the maximum discharge capacity at the drain step is larger than the actual discharge quantity as follows.

(Actual CO_2 discharge quantity per a cycle)< (S1)
(maximum CO_2 discharge capacity per volume)(total bed volume)

Each term in Eq. (S1) is given

(Actual CO_2 discharge quantity per a cycle)
=(mean CO_2 discharge flow)(total cycle time) (S2)
$$=\frac{(\text{flow of } CO_2 \text{ feed})(CO_2 \text{ recovery})}{(\text{Heavy flow recycle ratio})}(\text{total cycle time})$$

(maximum CO_2 discharge capacity per volume)
$=\rho_B(q_{CO_2}$ at the start of drain step
$-q_{CO_2}$ at the end of drain step) (S3)
$+\varepsilon_B(C_{CO_2}$ at the start of drain step
$-C_{CO_2}$ at the end of drain step)

where ρ_B is the bed density, q_{CO_2} is the adsorption amount of CO_2, ε_B is bed porosity and C_{CO_2} is the molar concentration of CO_2.

$$(\text{total bed volume})=\left(\frac{\text{total cycle time}}{\text{feeding time}}\right)(\text{unit bed volume}) \quad \text{(S4)}$$

Therefore, the minimum required volume can be calculated at the drain step.

$$(\text{minimum total bed volume})_{drain}=\frac{(\text{mean } CO_2 \text{ discharge flow})(\text{total cycle time})}{(\text{maximum } CO_2 \text{ discharge capacity per volume})} \quad \text{(S5)}$$

$$(\text{minmimum unit bed volume})_{drain}=\frac{(\text{mean } CO_2 \text{ discharge flow})(\text{feeding time})}{(\text{maximum } CO_2 \text{ discharge capacity per volume})} \quad \text{(S6)}$$

As a result, the larger size bed is required if the cycle time increases or the CO_2 discharge capacity decreases. Reynolds et al. [14, 15] reported that the PSA performance was improved as the cycle time increases. Thus, to improve the PSA performance, the bed size should increase as well. The CO_2 discharge capacity is determined by the pressure change of the drain step. The complex PSA sequence having multiple pressure equalization steps [8] and the drain after the depressurization step [15] causes low pressure drops at the drain step. Then, the discharge quantity per cycle becomes smaller and the bed size should be larger for a given design capacity.

The determination of the bed size for the feeding step can be done in a way similar to the previous calculation for the drain step. If the repressurization is performed by a feed gas stream, both repressurization and adsorption steps are included in the feeding step.

(Actual CO_2 adsorption quantity per a bed)< (S7)
(maximum CO_2 adsorption capacity per volume)(unit bed volume)

(Actual CO_2 adsorption quantity per a bed)
=(mean CO_2 adsorption rate)(total feeding time) (S8)
$=\eta_{ads}$(flow of CO_2 feed)(total feeding time)

η_{ads} is the adsorption efficiency, which is the ratio of the adsorbed amount of CO_2 to the total amount of CO_2 injection during the feeding step. If the purge reflux is not high, η_{ads} is equivalent to CO_2 recovery.

(maximum CO_2 adsorption capacity per volume)
$=\rho_B(q_{CO_2}$ at the start of feeding step-q_{CO_2} at the end of feding step) (S9)
$+\varepsilon_B(C_{CO_2}$ at the start of feeding step-C_{CO_2} at the end of feeding step)

$$(\text{minimum total bed volume})_{feeding}=\frac{(\text{mean } CO_2 \text{ adsorption rate})(\text{total cycle time})}{(\text{maximum } CO_2 \text{ adsorption capacity per volume})} \quad \text{(S10)}$$

$$(\text{minimum unit bed volume})_{feeding}=\frac{(\text{mean } CO_2 \text{ adsorption rate})(\text{feeding time})}{(\text{maximum } CO_2 \text{ adsorption capacity per volume})} \quad \text{(S11)}$$

The required bed size for the feeding step increases as the total cycle time increases or the CO_2 adsorption capacity decreases. The CO_2 influxes prior to the feeding step from the pressure equalization and reflux purge steps lead to a decline of CO_2 adsorption capacity in the feeding step.

The calculation result for Case 5 is summarized in Table S3. The

Table S3. Required bed volumes for the purge-EQ sequence in Case 5

Step	CO_2 feed rate	CO_2 recovery	Feeding time	Total cycle time	Recycle ratio	CO_2 discharge (adsorption) capacity	Required volume	Required volume per CO_2 product
	mol/s	-	s	s	-	mol/m^3	cm^3	m^3/(kmol CO_2/s)
Feeding	6.15e-3	0.766	85	255	-	85.89	(unit bed) 466	(unit bed) 99
							(total bed) 1399	(total bed) 297
Drain	6.15e-3	0.766	85	255	0.61	111.87	(unit bed) 586	(unit bed) 124
							(total bed) 1758	(total bed) 373

required bed size for the drain step is larger than the bed size required for the feeding. As a result, the bed size is determined by the CO_2 discharge amount at the drain step. Our proposed design of each single step of CO_2-rich gas purge and pressure equalization is the most efficient for pre-combustion CCS. Thus, we may find the best combination of purge and pressure equalization steps to increase the PSA performance. It is not certain that more complex processes improved the PSA performance because complex PSA sequences cause the increase in the bed size. For example, the bed size required for the 5-bed and 5-step PSA sequence [15] is about 50,000 m^3/(kmol CO_2/s) which is much larger than the total bed size required for our proposed sequence of sequential pressure equalization and purge steps (373 m^3/(kmol CO_2/s) in Table S3).